An unknown input observer based control allocation scheme for icing diagnosis and accommodation in overactuated UAVs

Andrea Cristofaro and Tor Arne Johansen

***Abstract*— The accretion of ice layers on wings and control surfaces modifies their lift and drag and, consequently, alters performance and controllability of the aircraft. In this paper we propose a combined unknown input observers and control allocation framework to design icing diagnosis filters and accommodate icing for an overactuated automated aircraft.**

I. Introduction

The efficiency and reliability of operations in isolated areas have significantly increased thanks to the development of advanced control systems and the use of automated vehicles. On the other hand, such systems are expected to face very critical and harsh conditions. Unmanned aerial vehicles (UAVs), whose employment as support to operations in remote environments is becoming more and more crucial, are naturally prone to the occurrence of icing. Detection and accommodation of ice adhesion on wings, control surfaces and sensors is a challenging and primary issue for UAVs, since the ice accretion modifies the shape of the aircraft and alters the measurements, this causing adverse changes on aerodynamic forces and reducing the maneuvring capabilities. The phenomenon of icing, that can be regarded as a structural fault, is a well recognized problem in aviation research since the early 1900s [1].

The formation of ice layers decrease the lift and, simultaneously, increase the drag and the mass of the vehicle, this requiring additional engine power and implying a premature stall angle [2]. Inflight icing is typically caused by the impact of supercooled water droplets (SWD). When a water droplet is cooled, it does not freeze until it reaches very low temperatures; however, if the droplet impact on the aircraft surface it freezes immediately and accretes ice [3]. The rate and the severity of icing are determined by several factors, such as shape and roughness of the impacting surface, vehicle speed, air temperature and relative humidity.

The consequences of icing are even more severe for small unmanned aircrafts due to their simple architecture and limited payload, this making them mostly unsuitable for the typical anti-icing and de-icing devices that are used in large airplanes. Small UAVs are also more prone to icing than most other aircrafts since they often operate at low altitude where high humidity and SWD are encountered more frequently. Larger aircraft tend to operate at high altitude (except for take off and landing) where there are less risks of icing. Some advanced de-icing systems for UAVs have been recently proposed based on layers of coating material made of carbon nanotubes [4] [5]. However, since these are very power consuming, in order to guarantee the efficiency of the system it is very important to rely on fault/icing detection schemes with fast and accurate responses. On the other hand, the availability of redundant control surfaces is a key advantage toward safe aircraft maneuvring and stability in spite of icing. Control allocation [6] is a very helpful setup, as it allows to handle constraints and incorporate secondary objectives in a straightforward way. Moreover, several results on CA-based fault detection/isolation and fault tolerant control have been recently proposed [7] [8] [9] [10].

Adopting some tools from the control allocation framework, in this paper we present an unknown input observer approach for icing diagnosis and accommodation in UAVs with a redundant suite of effectors. This work started with [11], where the problem of icing detection has been addressed considering the linearized longitudinal model of the vehicle. A similar approach for the lateral dynamics has been previously proposed in [12], while further improvements have been obtained using multiple-models [13] and LPV methods [14] [15]. The novel contribution in this paper is the generalization of the architecture introduced in [11] to the linear 6-DOF motion model with coupled longitudinal/lateral dynamics, and the integration with a fault-tolerant allocation scheme for accommodating effector faults and with a carbon-nanotubes automated system for the inflight de-icing of the airfoils. The paper is structured as follows. The UAV model and the basic setup are given in Section II, while the icing effects are discussed in Section III. Section IV and V are, respectively, dedicated to present the icing diagnosis and icing accommodation tasks. Finally, a simulation study is proposed in Section VI.

II. Vehicle model and basic setup

Let us consider the 6-DOF aircraft nonlinear model [16], consisting of three equations for velocity components $(\tilde{u}, \tilde{v}, \tilde{w})$, three equations for attitude $(\tilde{\phi}, \tilde{\theta}, \tilde{\psi})$ and three equations for moments $(\tilde{p}, \tilde{q}, \tilde{r})$

$$
\begin{aligned}
m\dot{\tilde{u}} &= m(\tilde{r}\tilde{v} - \tilde{q}\tilde{w} - g\sin\tilde{\theta}) + \mathcal{A}_x + \mathcal{T} \\
m\dot{\tilde{v}} &= m(\tilde{p}\tilde{w} - \tilde{r}\tilde{u} + g\cos\tilde{\theta}\sin\tilde{\phi}) + \mathcal{A}_y \\
m\dot{\tilde{w}} &= m(\tilde{q}\tilde{u} - \tilde{p}\tilde{v} + g\cos\tilde{\theta}\cos\tilde{\phi}) + \mathcal{A}_z \\
\dot{\tilde{\phi}} &= \tilde{p} + \tilde{q}\sin\tilde{\phi}\tan\tilde{\theta} + \tilde{r}\cos\tilde{\phi}\tan\tilde{\theta} \\
\dot{\tilde{\theta}} &= \tilde{q}\cos\tilde{\phi} - \tilde{r}\sin\tilde{\phi} \\
\dot{\tilde{\psi}} &= \tilde{q}\sin\tilde{\phi}\sec\tilde{\theta} + \tilde{r}\cos\tilde{\phi}\sec\tilde{\theta}
\end{aligned}
$$

A. Cristofaro and T.A. Johansen are with Center for Autonomous Marine Operations and Systems (NTNU–AMOS) and with Department of Engineering Cybernetics, Norwegian University of Science and Technology , Norway. email: andrea.cristofaro@itk.ntnu.no, tor.arne.johansen@itk.ntnu.no

This work is part of the work carried out at AMOS. It is supported by the Research Council of Norway through the Centres of Excellence funding scheme, project No. 223254 - NTNU–AMOS.

$$\begin{aligned}\dot{\tilde{p}} &= \Gamma_1\tilde{p}\tilde{q} - \Gamma_2\tilde{q}\tilde{r} + \mathcal{M}_p\\ \dot{\tilde{q}} &= \Gamma_5\tilde{p}\tilde{r} - \Gamma_6(\tilde{p}^2 - \tilde{r}^2) + \mathcal{M}_q\\ \dot{\tilde{r}} &= \Gamma_7\tilde{p}\tilde{q} - \Gamma_1\tilde{q}\tilde{r} + \mathcal{M}_r\end{aligned}$$

where m is vehicle mass, $\mathcal{A}_i$ are aerodynamical forces (lift and drag), $\mathcal{T}$ is the thrust force, $\mathcal{M}_i$ are aerodynamical torques, and Γ_i are coefficients obtained as combinations of the main inertia coefficient I_{xx}, I_{yy}, I_{zz} and I_{xz}.. The velocities $\tilde{u}, \tilde{v}, \tilde{w}$ are expressed in the body frame, i.e. along longitudinal, lateral and vertical body direction respectively, and they represent the aircraft velocity relative to the wind.

In order to simplify the analysis, consider a suitable trim condition $x^* := (u^*, v^*, w^*, \phi^*, \theta^*, \psi^*, p^*, q^*, r^*)$ and linearize the above system as follows. Setting

$$\begin{aligned}&u := \tilde{u} - u^*,\ v := \tilde{v} - v^*,\ w := \tilde{w} - w^*\\ &\phi := \tilde{\phi} - \phi^*,\ \theta := \tilde{\theta} - \theta^*,\ \psi := \tilde{\psi} - \psi^*\\ &p := \tilde{p} - p^*,\ q := \tilde{q} - q^*,\ r := \tilde{r} - r^*\end{aligned}$$

one obtains a 6-DOF linear system describing the linearized coupled longitudinal/lateral dynamics of the aircraft:

$$\dot{\mathbf{x}} = \mathbf{A}\mathbf{x} + \mathbf{B}\boldsymbol{\tau} \tag{1}$$

with $\mathbf{x} := [u, v, w, \phi, \theta, \psi, p, q, r]^T$, $\boldsymbol{\tau} = [\tau_t, \tau_e, \tau_a, \tau_r]^T$ and

$$\mathbf{A} = \begin{bmatrix} X_u & X_v & X_w & 0 & X_\theta & 0 & 0 & X_q & X_r\\ Y_u & Y_v & Y_w & Y_\phi & Y_\theta & 0 & Y_p & 0 & Y_r\\ Z_u & Z_v & Z_w & Z_\phi & Z_\theta & 0 & Z_p & Z_q & 0\\ 0 & 0 & 0 & \Phi_\phi & \Phi_\theta & 0 & \Phi_p & \Phi_q & \Phi_r\\ 0 & 0 & 0 & \Theta_\phi & 0 & 0 & 0 & \Theta_q & \Theta_r\\ 0 & 0 & 0 & \Psi_\phi & \Psi_\theta & 0 & 0 & \Psi_q & \Psi_r\\ L_u & L_v & L_w & 0 & 0 & 0 & L_p & L_q & L_r\\ M_u & M_v & M_w & 0 & 0 & 0 & M_p & M_q & M_r\\ N_u & N_v & N_w & 0 & 0 & 0 & N_p & N_q & N_r \end{bmatrix}$$

$$\mathbf{B} = \begin{bmatrix} X_{\tau_t} & X_{\tau_e} & 0 & 0\\ 0 & 0 & Y_{\tau_a} & Y_{\tau_r}\\ 0 & Z_{\tau_e} & 0 & 0\\ 0 & 0 & 0 & 0\\ 0 & 0 & 0 & 0\\ 0 & 0 & 0 & 0\\ 0 & 0 & L_{\tau_a} & L_{\tau_r}\\ 0 & M_{\tau_e} & 0 & 0\\ 0 & 0 & N_{\tau_a} & N_{\tau_r} \end{bmatrix}$$

The coefficients for airspeed and angular moments $X_i, Y_i, Z_i, L_i, M_i, N_i$, $i = u, v, w, p, q, r, \tau_e, \tau_a, \tau_r$, depend on the dynamic pressure ρ, the wing surface area S, the airfoil chord c, the wing span b and some coefficients $C_{\sharp_i}$, $\sharp = X, Y, Z, L, M, N$, that are specific for any aircraft: these are usually referred to as control and stability derivatives. The control inputs are the propeller angular speed τ_t and the surface deflections τ_e, τ_a and τ_r producing torques. In this paper, without loss of generality, the aircraft is supposed to be a V-tail vehicle [16], and hence the redundancy of control surfaces is expressed by the linear effector model:

$$\boldsymbol{\tau} = \mathbf{G}\boldsymbol{\delta}, \quad \boldsymbol{\delta} := \begin{bmatrix} \tau_t \\ \boldsymbol{\delta}_1 \end{bmatrix} \tag{2}$$

where $\boldsymbol{\delta}_1 \in \mathbb{R}^4$ is a vector incorporating left and right aileron deflections, and left and right rudder deflections:

$$\boldsymbol{\delta}_1 = \begin{bmatrix} \delta_{al} \\ \delta_{ar} \\ \delta_{rl} \\ \delta_{rr} \end{bmatrix}$$

In particular, a pitching moment is induced when moving the ailerons jointly, while moving them alternatively produces a rolling moment. Similarly, yawing moment is induced by an alternative movement of elevons, while a joint movement produces a pitching moment. The matrix $\mathbf{G} \in \mathbb{R}^{4\times5}$ is assigned by

$$\mathbf{G} = \begin{bmatrix} 1 & 0 & 0 & 0 & 0\\ 0 & \epsilon & \epsilon & 1 & 1\\ 0 & \frac{1}{2} & -\frac{1}{2} & 0 & 0\\ 0 & 0 & 0 & 1 & -1 \end{bmatrix},$$

where the parameter $\epsilon > 0$ is inverse proportional to the distance between the aircraft center of gravity (usually assumed aligned with wings) and the tail.

The system is supposed to be equipped with a sensor suite including a pitot static tube aligned with the longitudinal body axis, a GPS, an altimeter, gyroscopes and accelerometers. The following main outputs $\mathbf{y} \in \mathbb{R}^7$ are therefore considered: horizontal airspeed $y_1 = \tilde{u}$, attitude angles $(y_2, y_3, y_4) = (\tilde{\phi}, \tilde{\theta}, \tilde{\psi})$ and angular velocities $(y_5, y_6, y_7) = (\tilde{p}, \tilde{q}, \tilde{r})$; according to the linearization and the trim of state variables, the output matrix $\mathring{\mathbf{C}} \in \mathbb{R}^{7\times9}$ associated to (1) turns out to be

$$\mathring{\mathbf{C}} := \begin{bmatrix} 1 & \mathbf{0}_{1\times2} & \mathbf{0}_{1\times6} \\ \mathbf{0}_{6\times1} & \mathbf{0}_{6\times2} & \boldsymbol{I}_{6\times6} \end{bmatrix} \tag{3}$$

In addition, the GPS and the altimeter provide position measurements $(\tilde{x}_N, \tilde{x}_E, \tilde{x}_D)$ expressed in the inertial frame; the position coordinates are assigned by the kinematic equations

$$\begin{bmatrix} \dot{\tilde{x}}_N \\ \dot{\tilde{x}}_E \\ \dot{\tilde{x}}_D \end{bmatrix} = \mathbf{R}\left(\tilde{\phi}, \tilde{\theta}, \tilde{\psi}\right) \begin{bmatrix} \tilde{u} \\ \tilde{v} \\ \tilde{w} \end{bmatrix} + \boldsymbol{\nu},$$

where the matrix $\mathbf{R}(\cdot,\cdot,\cdot)$ represents the rotation from body to inertial frame and $\boldsymbol{\nu} = [\nu_N\ \nu_E\ \nu_D]^T$ is the wind speed (expressed in the inertial frame). We notice that, whenever an accurate wind speed estimator is available [17] [18], the interpolation of the estimated wind speed with the average aircraft speed, that can be computed through the GPS data, provides also a measurement of the relative velocities v, w and hence in this case one can rely on an output matrix $\bar{\mathbf{C}} \in \mathbb{R}^{9\times9}$. We will refer to $\mathbf{C} = \bar{\mathbf{C}}$ as to *full information case* and to $\mathbf{C} = \mathring{C}$ as to *partial information case*.

The system is supposed to be controlled by an autopilot responsible to produce the desired control effect $\boldsymbol{\tau}_c$, that is typically provided by a suitable controller. The generation of the desired control effect is distributed over the redundant effectors according to (2), in particular the control allocation module is in charge to determine $\boldsymbol{\delta}_c$ such that

$$\boldsymbol{\tau}_c = \mathbf{G}\boldsymbol{\delta}_c.$$

The airspeed dynamics is affected by the wind effect, that can be expressed by the additional input

$$-\mathbf{R}\left(\tilde{\phi},\tilde{\theta},\tilde{\psi}\right)\dot{\boldsymbol{\nu}}$$

where $\dot{\boldsymbol{\nu}} = [\dot{\nu}_N\ \dot{\nu}_E\ \dot{\nu}_D]^T$ is the wind acceleration expressed in the inertial frame. The wind $\boldsymbol{\nu}$ is typically decomposed as the sum of a steady component (known or accurately estimated) $\boldsymbol{\nu}^*$ with $\dot{\boldsymbol{\nu}}^* = 0$ and a turbulence component $\boldsymbol{\nu}^{\vdash}$: this leads to an input disturbance $\boldsymbol{\xi}(t) \in \mathbb{R}^9$ given by

$$\boldsymbol{\xi}(t) = \mathbf{N}(t)\begin{bmatrix} \dot{\nu}_N^{\vdash} \\ \dot{\nu}_E^{\vdash} \\ \dot{\nu}_D^{\vdash} \end{bmatrix},\ \mathbf{N}(t) := \begin{bmatrix} -\mathbf{R}\left(\tilde{\phi},\tilde{\theta},\tilde{\psi}\right) \\ \mathbf{0}_{6\times 3} \end{bmatrix} \quad (4)$$

Summarizing, combining (1)-(4), we have to deal with the following uncertain linear plant

$$\begin{aligned} \dot{\mathbf{x}} &= \mathbf{A}\mathbf{x} + \mathbf{B}\mathbf{G}\boldsymbol{\delta} + \mathbf{N}\dot{\boldsymbol{\nu}}^{\vdash} \\ \mathbf{y} &= \mathbf{C}\mathbf{x} \end{aligned} \quad (5)$$

where $\mathbf{N} = \mathbf{N}(t)$ is a time-varying input matrix.

III. Icing effect model

The accretion of clear ice on the aircraft surfaces modifies stability and control derivatives according to the following linear model [19]

$$C_{\sharp i}^{ice} = (1 + \eta\mathcal{K}_{\sharp i})C_{\sharp i}, \quad \begin{matrix} \sharp = X, Y, Z, L, M, N \\ i = u, v, w, p, q, r, \tau_e, \tau_a, \tau_r \end{matrix} \quad (6)$$

where η is the icing severity factor and the coefficient $\mathcal{K}_{\sharp}$ depends on aircraft specifications [19]; the clean condition corresponds to $\eta = 0$, while the all iced condition occurs for $\eta = \eta_{\max}$ [2]. Such model has been developed on the basis of real data obtained from different icing encounters [19]. The overall effect of icing can be modeled as an additive disturbance term $\eta\boldsymbol{\omega}$, where η is a scalar unknown quantity and the vector $\boldsymbol{\omega}$ is assigned by

$$\boldsymbol{\omega} = \mathbf{A}_{\mathcal{E}}\mathbf{x} + \mathbf{B}_{\mathcal{E}}\boldsymbol{\tau}$$

with

$$\mathbf{A}_{\mathcal{E}} = \begin{bmatrix} \mathcal{E}_{X_u} & \mathcal{E}_{X_v} & \mathcal{E}_{X_w} & 0 & 0 & 0 & 0 & \mathcal{E}_{X_q} & 0 \\ \mathcal{E}_{Y_u} & \mathcal{E}_{Y_v} & \mathcal{E}_{Y_w} & 0 & 0 & 0 & \mathcal{E}_{Y_p} & 0 & \mathcal{E}_{Y_r} \\ \mathcal{E}_{Z_u} & \mathcal{E}_{Z_v} & \mathcal{E}_{Z_w} & 0 & 0 & 0 & 0 & \mathcal{E}_{Z_q} & 0 \\ 0 & 0 & 0 & 0 & 0 & 0 & 0 & 0 & 0 \\ 0 & 0 & 0 & 0 & 0 & 0 & 0 & 0 & 0 \\ 0 & 0 & 0 & 0 & 0 & 0 & 0 & 0 & 0 \\ \mathcal{E}_{L_u} & \mathcal{E}_{L_v} & \mathcal{E}_{L_w} & 0 & 0 & 0 & \mathcal{E}_{L_p} & 0 & \mathcal{E}_{L_r} \\ \mathcal{E}_{M_u} & \mathcal{E}_{M_v} & \mathcal{E}_{M_w} & 0 & 0 & 0 & 0 & \mathcal{E}_{M_q} & 0 \\ \mathcal{E}_{N_u} & \mathcal{E}_{N_v} & \mathcal{E}_{N_w} & 0 & 0 & 0 & \mathcal{E}_{N_p} & 0 & \mathcal{E}_{N_r} \end{bmatrix}$$

$$\mathbf{B}_{\mathcal{E}} = \begin{bmatrix} 0 & \mathcal{E}_{X_{\tau_e}} & 0 & 0 \\ 0 & 0 & \mathcal{E}_{Y_{\tau_a}} & \mathcal{E}_{Y_{\tau_r}} \\ 0 & \mathcal{E}_{Z_{\tau_e}} & 0 & 0 \\ 0 & 0 & 0 & 0 \\ 0 & 0 & 0 & 0 \\ 0 & 0 & 0 & 0 \\ 0 & 0 & \mathcal{E}_{L_{\tau_a}} & \mathcal{E}_{L_{\tau_r}} \\ 0 & \mathcal{E}_{M_{\tau_e}} & 0 & 0 \\ 0 & 0 & \mathcal{E}_{N_{\tau_a}} & \mathcal{E}_{N_{\tau_r}} \end{bmatrix}$$

where the coefficients $\mathcal{E}_{\sharp}$ are obtained from $\mathcal{K}_{\sharp}$ and $C_{\sharp}$ by performing linear combinations. The icing severity factor evolves according to the law

$$\eta = \mathcal{N}(\varpi)\cdot\chi$$

where $\mathcal{N}(\cdot)$ is a nonlinear function, ϖ is the fraction of water freezing at a point on a surface to the water impinging on the surface,

$$\varpi = \frac{\text{mass of water freezing}}{\text{mass of water impinging}},$$

and $\chi \geq 0$ is the accumulation parameter defined as the mass flux [20]

$$\dot{\chi} = \frac{e\lambda F_a}{\varrho c}(1 - \iota_{airfoil}), \quad (7)$$

e being the collection efficiency, λ the liquid water content, F_a is the free stream velocity, ϱ the ice density, c is the airfoil chord and $\iota_{airfoil} \in [0,1]$ is the airfoil icing protection coefficient. Both the fraction ϖ and the ice density ρ depend on the air temperature and the relative humidity. In particular, when the temperature is below $-10°C$ the factor ϖ satisfies $\varpi \approx 1$, this corresponding to rime ice formation; on the other hand, if the temperature is between $-10°C$ and $0°C$, glaze ice typically appears with $\varpi < 1$. On the other hand, due to aerodynamical cooling effects, icing can also occur when the outside air temperature is close to freezing point but still warmer than $0°$. It has been observed experimentally [19] that the icing severity factor achieves its maximum $\eta_{\max}$ when the freezing fraction ϖ is close to the value $\varpi_g = 0.2$, while it decreases to a steady value as ϖ approaches 1.
Icing can also impact on the aircraft maneuverability by decreasing the effectiveness of control surfaces. Assume that the effector position is driven by the dynamical relationships

$$\dot{\delta}_{\flat} = f_{\flat}(\delta_{\flat}, \gamma_{\flat}), \quad \flat = al, ar, rl, rr,$$

where $\gamma_{\flat}$ is the actuator input and the vector field $f(\cdot,\cdot)$ is supposed to be asymptotically stable for the free dynamics $\dot{\delta}_{\flat} = f_{\flat}(\delta_{\flat}, 0)$. The presence of ice may cause malfunctions of actuators and surface blockage; the effects can be generally modeled as the combination of loss of efficiency multiplicative factors $d_{\flat}(t)$ and additive factors $\varphi_{\flat}$:

$$\dot{\delta}_{\flat} = d_{\flat}f_{\flat}(\delta_{\flat}, \gamma_{\flat}) + \varphi_{\flat}, \quad \flat = al, ar, rl, rr \quad (8)$$

$$\begin{aligned} d_{\flat} &= 1 && t \leq t_0 \\ d_{\flat} &\in [0,1) && t > t_0 \\ \varphi_{\flat} &\neq 0 && t \geq t_0' \end{aligned} \quad (9)$$

We notice that the same model catches also the effects of electrical or mechanical faults that may occur in effectors and actuators. For this reason, throughout the paper, we will refer to model (8)-(9) as a generic effector fault.

IV. Icing diagnosis using Unknown Input Observers

This section is devoted to the design of a Fault Diagnosis scheme able to detect the icing and to identify whether the presence of ice on a particular control surface is causing a loss of effectiveness of the surface itself, or the ice accretion

on the leading edge of the wings and tail is causing a change of the airfoils aerodynamical properties. The method is to design the FD scheme based on Unknown Input Observers with constrained output directions [21] [11]. Unknown Input Observers is a well established and helpful tool for robust fault detection, and they have already been studied in the flight fault diagnosis framework [22] [23]. Let us consider

$$\mathbf{G} = [\mathbf{G_1}\ \mathbf{G_2}\ \mathbf{G_3}\ \mathbf{G_4}\ \mathbf{G_5}]$$

and set $\mathbf{W} = \mathbf{BG}$ with

$$\mathbf{W} = [\mathbf{W_1}\ \mathbf{W_2}\ \mathbf{W_3}\ \mathbf{W_4}\ \mathbf{W_5}].$$

Consider a generic linear UIO assigned by the equations

$$\begin{aligned}\dot{\mathbf{z}} &= \mathbf{Fz} + \mathbf{SB}\boldsymbol{\tau_c} + \mathbf{Ky}\\ \hat{\mathbf{x}} &= \mathbf{z} + \mathbf{Hy}\end{aligned}$$

where $\boldsymbol{\tau}_c$ is the (nominal) commanded input, and assume that the observer matrices are designed such that the following conditions are met

$$\mathbf{K} = \mathbf{K_1} + \mathbf{K_2} \tag{10}$$
$$\mathbf{S} = \mathbf{I} - \mathbf{HC} \tag{11}$$
$$\mathbf{F} = \mathbf{SA} - \mathbf{K_1C}, \quad \sigma(\mathbf{F}) \in \mathbb{C}^- \tag{12}$$
$$\mathbf{K_2} = \mathbf{FH} \tag{13}$$

where $\mathbf{C}$ is the output matrix of the system. The matrix $\mathbf{H} \in \mathbb{R}^{9\times p}$, with either $p = 9$ or $p = 7$, is a free design parameter that can be tuned in order to assign desired directions to residuals and to decouple them from unknown input disturbances. The two cases of full and partial information have to be treated separately.

A. Full information case

Let us consider the case $\mathbf{C} = \bar{\mathbf{C}}$ first. Let us select three linearly independent and constant vectors $\mathbf{N}_1, \mathbf{N}_2, \mathbf{N}_3 \in \mathbb{R}^9$ with

$$span\{\mathbf{N}_1, \mathbf{N}_2, \mathbf{N}_3\} = span\mathbf{N}(t) \quad \forall t \geq 0.$$

The basic idea is to make the residuals independent on the three components of the wind force, and to assign a particular output directions to each of the four input vectors corresponding to control surfaces (not including the engine throttle input vector $\mathbf{W_1}$). This is expressed by the identities

$$\bar{\mathbf{C}}(\mathbf{I} - \mathbf{H}\bar{\mathbf{C}})\mathbf{N_i} = 0, \qquad i = 1, 2, 3 \tag{14}$$
$$\bar{\mathbf{C}}(\mathbf{I} - \mathbf{H}\bar{\mathbf{C}})\mathbf{W_{i+1}} = \mathbf{e_i}, \quad i = 1, 2, 3, 4, \tag{15}$$

where $\mathbf{e_i}$ is the i^{th} vector of the standard basis in the output space $\mathbb{R}^7$. On the other hand, the four conditions (15) cannot be imposed simultaneously due to the lack of rank of the matrix $\mathbf{G}$, and we have to limit to consider three of them. To design such matrix $\mathbf{H}$ one can proceed as follows. Select a set of three independent vectors in $\mathbb{R}^9$, namely $\{\mathbf{b_1}, \mathbf{b_2}, \mathbf{b_3}\}$, such that

$$\bar{\mathbf{C}}\mathbf{b_i} = \mathbf{e_i} \quad i = 1, 2, 3.$$

Setting $\boldsymbol{\Upsilon} = [\mathbf{0}\ \mathbf{0}\ \mathbf{0}\ \mathbf{b_1}\ \mathbf{b_2}\ \mathbf{b_3}]$ and $\boldsymbol{\Lambda_{234}} = [\mathbf{N_1}\ \mathbf{N_2}\ \mathbf{N_3}\ \mathbf{W_2}\ \mathbf{W_3}\ \mathbf{W_4}]$ with $\boldsymbol{\Upsilon}, \boldsymbol{\Lambda_{234}} \in \mathbb{R}^{9\times 6}$ a simple solution is given by

$$\mathbf{H_{234}} = (\boldsymbol{\Lambda_{234}} - \boldsymbol{\Upsilon})(\bar{\mathbf{C}}\boldsymbol{\Lambda_{234}})^{-\mathbf{L}},$$

where $(\cdot)^{-L}$ stands for the left-pseudo inverse of a matrix. Choosing a different combination, say $\boldsymbol{\Lambda_{345}} = [\mathbf{N_1}\ \mathbf{N_2}\ \mathbf{N_3}\ \mathbf{W_3}\ \mathbf{W_4}\ \mathbf{W_5}]$, a second solution is found

$$\mathbf{H_{345}} = (\boldsymbol{\Lambda_{345}} - \boldsymbol{\Upsilon})(\bar{\mathbf{C}}\boldsymbol{\Lambda_{345}})^{-\mathbf{L}}.$$

Summarizing, we have two distinct UIOs, whose estimated states $\hat{\mathbf{x}}^{(1)}, \hat{\mathbf{x}}^{(2)}$ satisfy

$$\dot{\mathbf{x}} - \dot{\hat{\mathbf{x}}}^{(1)} = \mathbf{F}^{(1)}(\mathbf{x} - \hat{\mathbf{x}}^{(1)}) + \mathbf{S}^{(1)}(\mathbf{N}\dot{\boldsymbol{\nu}} + \mathbf{BG}\tilde{\boldsymbol{\delta}} + \eta\boldsymbol{\omega}) \tag{16}$$
$$\dot{\mathbf{x}} - \dot{\hat{\mathbf{x}}}^{(2)} = \mathbf{F}^{(2)}(\mathbf{x} - \hat{\mathbf{x}}^{(2)}) + \mathbf{S}^{(2)}(\mathbf{N}\dot{\boldsymbol{\nu}} + \mathbf{BG}\tilde{\boldsymbol{\delta}} + \eta\boldsymbol{\omega}) \tag{17}$$

where the matrices are defined as

$$\mathbf{F}^{(\mathrm{i})} = \mathbf{S}^{(\mathrm{i})}\mathbf{A} - \mathbf{K}_1^{(\mathrm{i})}\bar{\mathbf{C}}, \quad i = 1, 2$$
$$\mathbf{S}^{(1)} = \mathbf{I} - \mathbf{H_{234}}\bar{\mathbf{C}}, \quad \mathbf{S}^{(2)} = \mathbf{I} - \mathbf{H_{345}}\bar{\mathbf{C}}$$
$$\mathbf{S}^{(1)}[\mathbf{W_2}\ \mathbf{W_3}\ \mathbf{W_4}] = \mathbf{S}^{(2)}[\mathbf{W_3}\ \mathbf{W_4}\ \mathbf{W_5}] = [\mathbf{b_1}\ \mathbf{b_2}\ \mathbf{b_3}]$$

and $\tilde{\boldsymbol{\delta}}$ is the deviation of the actual control inputs from the commanded inputs

$$\tilde{\boldsymbol{\delta}} = \boldsymbol{\delta} - \boldsymbol{\delta}_c, \text{ with } \mathbf{G}\boldsymbol{\delta_c} = \boldsymbol{\tau_c}.$$

The key point of the construction is the selection of the matrix $\mathbf{K}_1^{(\mathrm{i})}$ $i = 1, 2$ in a way that $\mathbf{F}^{(i)}$ is Hurwitz with the triple $\{\mathbf{b_1}, \mathbf{b_2}, \mathbf{b_3}\}$ included in the set of its eigenvectors. This can be easily addressed by choosing an arbitrary Hurwitz matrix $\mathbf{M}^{(i)}$ having $\{\mathbf{b_1}, \mathbf{b_2}, \mathbf{b_3}\}$ as eigenvectors and setting

$$\mathbf{K}_1^{(\mathrm{i})} = (\mathbf{S}^{(i)}\mathbf{A} - \mathbf{M}^{(i)})\bar{\mathbf{C}}^{-1}. \tag{18}$$

The icing identification can be performed combining the two observers, i.e. defining a suitable logic to gather information from residual directions. Let use denote by $\bar{\mathbf{\Pi}}_i$ the linear projection operator on the subspace $span\{\mathbf{e}_i\} \subset \mathbb{R}^9, i = 1, ..., 9$, e.g.

$$\begin{aligned}\bar{\mathbf{\Pi}}_1 &= diag(1,0,0,0,0,0,0,0,0)\\ \bar{\mathbf{\Pi}}_2 &= diag(0,1,0,0,0,0,0,0,0)\\ &\vdots\\ \bar{\mathbf{\Pi}}_9 &= diag(0,0,0,0,0,0,0,0,1).\end{aligned}$$

Proposition 4.1: Set $\boldsymbol{\epsilon}^{(i)} = \bar{\mathbf{C}}(\mathbf{x} - \hat{\mathbf{x}}^{(\mathrm{i})})$, $i = 1, 2$. Assume estimator transients due to initial conditions to be negligible, i.e. $\boldsymbol{\epsilon}^{(i)}(0) = 0$. Then we can state the following decision rule.

- $\bar{\mathbf{\Pi}}_1\boldsymbol{\epsilon}^{(1)} = \boldsymbol{\epsilon}^{(1)} \neq 0 \Rightarrow$ *faulty effector* δ_{al}
- $\left\{\begin{array}{l}\bar{\mathbf{\Pi}}_2\boldsymbol{\epsilon}^{(1)} = \boldsymbol{\epsilon}^{(1)} \neq 0\\ \bar{\mathbf{\Pi}}_1\boldsymbol{\epsilon}^{(2)} = \boldsymbol{\epsilon}^{(2)} \neq 0\end{array}\right\} \Rightarrow$ *faulty effector* δ_{ar}
- $\left\{\begin{array}{l}\bar{\mathbf{\Pi}}_3\boldsymbol{\epsilon}^{(1)} = \boldsymbol{\epsilon}^{(1)} \neq 0\\ \bar{\mathbf{\Pi}}_2\boldsymbol{\epsilon}^{(2)} = \boldsymbol{\epsilon}^{(2)} \neq 0\end{array}\right\} \Rightarrow$ *faulty effector* δ_{rl}
- $\bar{\mathbf{\Pi}}_3\boldsymbol{\epsilon}^{(2)} = \boldsymbol{\epsilon}^{(2)} \neq 0 \Rightarrow$ *faulty effector* δ_{rr}
- $\bar{\mathbf{\Pi}}_j\boldsymbol{\epsilon}^{(i)} \neq \boldsymbol{\epsilon}^{(i)}\ \forall i = 1, 2\ \forall j = 1, 2, 3 \Rightarrow$ *airfoil icing*

Proof: Suppose that one effector is undergoing to a loss of efficiency due to icing or a mechanical malfunction, say δ_{ar} without loss of generality. By construction this means that

$$\mathbf{G}\tilde{\boldsymbol{\delta}} = \mathbf{G}_3\tilde{\delta}_{ar} \neq 0\ t \geq t_0.$$

Integration of (16)-(17) yields the residual evolution

$$\begin{aligned}\boldsymbol{\epsilon}^{(i)}(t) &= \bar{\mathbf{C}}\int_{t_0}^{t} e^{\mathbf{F}^{(i)}(t-\varsigma)}\mathbf{S}^{(i)}(\mathbf{N}(\varsigma)\dot{\boldsymbol{\nu}}(\varsigma)+\mathbf{B}\mathbf{G}_3\tilde{\delta}_{ar}(\varsigma))d\varsigma \\ &= \bar{\mathbf{C}}\int_{t_0}^{t} e^{\mathbf{F}^{(i)}(t-\varsigma)}\mathbf{S}^{(i)}\mathbf{W}_3\tilde{\delta}_{ar}(\varsigma)d\varsigma\end{aligned}$$

where the identity $\mathbf{S}^{(i)}\mathbf{N}(t)=0\ \forall t\geq 0$ has been used, and hence the residuals are decoupled from wind disturbances. Moreover, by (18) one has

$$\begin{aligned}\int_{t_0}^{t} e^{\mathbf{F}^{(1)}(t-\varsigma)}\mathbf{S}^{(1)}\mathbf{W}_3\tilde{\delta}_{ar}(\varsigma)d\varsigma &= \int_{t_0}^{t} e^{\lambda_2^{(1)}(t-\sigma)}\mathbf{b_2}\tilde{\delta}_{ar}(\varsigma)d\varsigma \\ &= \varphi_1(t)\mathbf{b_2}\end{aligned}$$

$$\begin{aligned}\int_{t_0}^{t} e^{\mathbf{F}^{(2)}(t-\varsigma)}\mathbf{S}^{(2)}\mathbf{W}_3\tilde{\delta}_{ar}(\varsigma)d\varsigma &= \int_{t_0}^{t} e^{\lambda_1^{(2)}(t-\sigma)}\mathbf{b_1}\tilde{\delta}_{ar}(\varsigma)d\varsigma \\ &= \varphi_2(t)\mathbf{b_1}\end{aligned}$$

for some scalar functions $\varphi_1(t),\ \varphi_2(t)$. Therefore, one gets

$$\boldsymbol{\epsilon}^{(1)}(t)=\varphi_1(t)\mathbf{e}_2,\quad \boldsymbol{\epsilon}^{(2)}(t)=\varphi_2(t)\mathbf{e}_1,$$

or equivalently

$$\bar{\mathbf{\Pi}}_2\boldsymbol{\epsilon}^{(1)}(t)=\boldsymbol{\epsilon}^{(1)}(t),\quad \bar{\mathbf{\Pi}}_1\boldsymbol{\epsilon}^{(2)}(t)=\boldsymbol{\epsilon}^{(2)}(t)\quad \forall t\geq t_0.$$

These two conditions allows us to identify the right aileron δ_{ar} as the faulty effector. The other cases of effector faults follow straightforwardly. On the other hand, in the presence of ice accreting on the wings for $t\geq t_{ice}$, the residuals $\boldsymbol{\epsilon}^{(i)}(t)$ will be not constantly oriented, in particular $\boldsymbol{\epsilon}^{(1)}(t)\in span\{\mathbf{e_1},\mathbf{e_2},\mathbf{e_3}\}$ for any $t\geq t_{ice}$, and hence the icing can be identified through the proposed decision algorithm. ■

Remark 4.1: The proposed decision rule can be extended to handle the case of multiple faults, i.e. the simultaneous failure of two effectors. The residuals turn out to be directed as combinations of two of the basis vectors, and hence the faulty devices can be still identified. However in this latter case, due rank deficiency, it is unlikely that exact control reconfiguration can be achieved by control allocation.

Remark 4.2: It is worth to note that only 6 of 9 outputs are effectively used in the proposed scheme, i.e. 3 degrees of freedom for zeroing the wind effects, and 3 degrees of freedom for assigning output directions to the columns of the matrix $\mathbf{W}$. Such dual redundancy may be used to enhance robustness of the algorithm in spite of sensor faults. As a matter of fact, icing may also occur on airspeed sensors, typically causing over-estimation of velocity; for this reason, in order to exclude possible biased airspeed measurements in the absence of probes equipped with heating devices, it might be safer to base the icing diagnosis method on a set of 6 outputs only, namely (ϕ,θ,ψ,p,q,r), even though in principle this might lead to a partial lack of observability in certain situations.

B. Partial information case

In the partial information case $\mathbf{C}=\mathring{\mathbf{C}}$ we have 7 independent outputs, and hence there are 7 directions that can be freely assigned. The construction is analogous to the full information case but, since $dim(span\{\mathring{\mathbf{C}}\mathbf{N}(\mathbf{t})\})=1$, there is no feasible way to design the observer being decoupled from wind accelerations in the lateral and vertical directions, namely $\dot{\nu}_y^{\vdash},\dot{\nu}_z^{\vdash}$. Similarly to the previous design procedure, we set

$$\begin{aligned}\mathbf{H_{234}} &= (\mathbf{\Lambda_{234}}-\mathbf{\Upsilon})(\mathring{\mathbf{C}}\mathbf{\Lambda_{234}})^{-\mathbf{L}}, \\ \mathbf{H_{345}} &= (\mathbf{\Lambda_{345}}-\mathbf{\Upsilon})(\mathring{\mathbf{C}}\mathbf{\Lambda_{345}})^{-\mathbf{L}}\end{aligned}$$

where the original matrices $\mathbf{\Lambda}$ and $\mathbf{\Upsilon}$ have been replaced by

$$\begin{aligned}\mathbf{\Lambda_{234}} &= [\mathbf{N_1}\ \mathbf{W_2}\ \mathbf{W_3}\ \mathbf{W_4}] \\ \mathbf{\Lambda_{345}} &= [\mathbf{N_1}\ \mathbf{W_3}\ \mathbf{W_4}\ \mathbf{W_5}] \\ \mathbf{\Upsilon} &= [\mathbf{0}\ \mathbf{b_1}\ \mathbf{b_2}\ \mathbf{b_3}],\end{aligned}$$

with $\mathbf{N_1}\in span\{\mathring{\mathbf{C}}\mathbf{N}(\mathbf{t})\}$. The following assumption, which is an extension of (18), guarantees that the eigenstructure of the matrices $\mathbf{F}^{(i)}$ can be assigned properly [24].

Assumption 4.1: A matrix $\mathbf{K_1^{(i)}}, i=1,2$, can be designed such that $\sigma(\mathbf{S^{(i)}A}-\mathbf{K_1^{(i)}}\mathring{\mathbf{C}})\in\mathbb{C}^-$ together with

$$\mathbf{F}^{(i)}\mathbf{b_j}=(\mathbf{S^{(i)}A}-\mathbf{K_1^{(i)}}\mathring{\mathbf{C}})\mathbf{b_j}=\lambda_{\mathbf{j}}^{(\mathbf{i})}\mathbf{b_j} \tag{19}$$

for some $\lambda_j^{(i)}<0$ and $j=1,2,3$.

A sufficient condition for the existence of a gain matrix $\mathbf{K_1^{(i)}}$ with the desired properties can be found in [21].

Let us denote by $\mathring{\mathbf{\Pi}}_i$ the linear projection operator on the subspace $span\{\mathbf{e}_i\}\subset\mathbb{R}^7, i=1,...,7$, e.g.

$$\begin{aligned}\mathring{\mathbf{\Pi}}_1 &= diag(1,0,0,0,0,0,0) \\ \mathring{\mathbf{\Pi}}_2 &= diag(0,1,0,0,0,0,0) \\ &\vdots \\ \mathring{\mathbf{\Pi}}_7 &= diag(0,0,0,0,0,0,1).\end{aligned}$$

In addition we denote by $\mathring{\mathbf{\Pi}}_i^{\perp}$ the projection operator on the subspace orthogonal to $span\{\mathbf{e}_i\}$. Since in this case the wind disturbances are not completely decoupled, we need to introduce suitable thresholds in the partial information isolation scheme. Suppose that bounds on the wind accelerations are available, i.e. $|\dot{\nu}_y^{\vdash}|\leq\vartheta_y,\quad |\dot{\nu}_z^{\vdash}|\leq\vartheta_z$. Set $\boldsymbol{\vartheta}=[0\ \vartheta_y\ \vartheta_z]^T$ and

$$\boldsymbol{\mu}^{(i)}(t)=\int_0^t e^{\mathbf{F}^{(i)}(t-\varsigma)}\mathbf{S}^{(i)}\boldsymbol{\vartheta}d\varsigma,$$

the latter being an upper bound for the forced response of residuals to wind disturbances.

The following result is a generalization of the rule stated in Proposition 4.1, where the identities have been replaced by inequalities in order to take into account model uncertainties and disturbances, these being no longer decoupled from residuals in the partial information case. The proof mimics the one of Proposition 4.1 and is therefore omitted.

Proposition 4.2: Set $\boldsymbol{\epsilon}^{(i)} = \mathring{\mathbf{C}}(\mathbf{x} - \hat{\mathbf{x}}^{(i)})$, $i = 1, 2$. *Assume estimator transients due to initial conditions to be negligible, i.e.* $\boldsymbol{\epsilon}^{(i)}(0) = 0$. *Then we can state the following decision rule for* $\boldsymbol{\epsilon}^{(i)} \neq 0$*:*

- $\|\mathring{\mathbf{\Pi}}_1 \epsilon^{(1)} - \epsilon^{(1)}\| \leq \|\mathring{\mathbf{\Pi}}_1^{\perp} \mu^{(1)}\| \Rightarrow$ *faulty effector* δ_{al}
- $\left.\begin{array}{l} \|\mathring{\mathbf{\Pi}}_2 \epsilon^{(1)} - \epsilon^{(1)}\| \leq \|\mathring{\mathbf{\Pi}}_2^{\perp} \mu^{(1)}\| \\ \|\mathring{\mathbf{\Pi}}_1 \epsilon^{(2)} - \epsilon^{(2)}\| \leq \|\mathring{\mathbf{\Pi}}_1^{\perp} \mu^{(2)}\| \end{array}\right\} \Rightarrow$ *faulty effector* δ_{ar}
- $\left.\begin{array}{l} \|\mathring{\mathbf{\Pi}}_3 \epsilon^{(1)} - \epsilon^{(1)}\| \leq \|\mathring{\mathbf{\Pi}}_3^{\perp} \mu^{(1)}\| \\ \|\mathring{\mathbf{\Pi}}_2 \epsilon^{(2)} - \epsilon^{(2)}\| \leq \|\mathring{\mathbf{\Pi}}_2^{\perp} \mu^{(2)}\| \end{array}\right\} \Rightarrow$ *faulty effector* δ_{rl}
- $\|\mathring{\mathbf{\Pi}}_3 \epsilon^{(2)} - \epsilon^{(2)}\| \leq \|\mathring{\mathbf{\Pi}}_3^{\perp} \mu^{(2)}\| \Rightarrow$ *faulty effector* δ_{rr}
- $\|\mathring{\mathbf{\Pi}}_j \epsilon^{(i)} - \epsilon^{(i)}\| > \|\mathring{\mathbf{\Pi}}_j^{\perp} \mu^{(i)}\| \ \forall i = 1, 2 \ \forall j = 1, 2, 3 \Rightarrow$ *airfoil icing*

Remark 4.3: In this case, the isolation of a fault is achieved when the difference between the residual $\epsilon^{(i)}$ and its projection on the direction $\mathbf{e}_j$ remains bounded by the projection of the wind acceleration threshold $\mu^{(i)}$ on the orthogonal subspace $\{\mathbf{e}_j\}^{\perp}$. A similar logic can be adopted to handle other types of system perturbations, such as model uncertainties or measurement noise. Moreover, a frequency separation approach with the introduction of additional filters may be helpful, since wind acceleration and sensor noise are high frequency disturbances while icing is characterized by a low frequency.

V. Icing accommodation

Once the icing has been detected, the control scheme is switched to some alarm mode. The alarm mode may be read as a reconfiguration in the case of effector icing [25] [7], or as the activation of an automated de-icing device in the case of accretion of ice on the leading edge of the wings [5]. Let us treat the two scenarios separately.

A. Effector icing: control reconfiguration

Suppose that one of the effectors has been identified as faulty or iced, say $\delta_{\flat^\star}$ with $\flat^\star \in \{al, ar, rl, rr\}$. Avoiding use of the effector $\delta_{\flat^\star}$ is desirable in order to prevent loss of control, and hence the corresponding actuator input $v_{\flat^\star}$ is set to zero in (8). However, due to the presence of the factor $d_{\flat^\star}$, this does not ensure that the state of $\delta_{\flat^\star}$ converges to zero [26]; in particular, denoting by $\Psi_{\flat^\star}(t, t_d)$ the solution of the free evolution equation (8) for t larger than the fault detection time t_d, one has

$$\lim_{t \to +\infty} \Psi_{\flat^\star}(t, t_d) = \bar{\delta}_{\flat^\star} \in \mathbb{R}, \quad \delta^{\dagger}_{\flat^\star}(t) := \Psi_{\flat^\star}(t, t_d) - \bar{\delta}_{\flat^\star}.$$

With a slight abuse of notation we indicate with $\mathbf{G}_{\flat^\star}$ the column of $\mathbf{G}$ corresponding to the faulty effector, and with $\breve{\boldsymbol{\delta}} \in \mathbb{R}^4$, $\breve{\mathbf{G}}_{\flat^\star} \in \mathbb{R}^{4 \times 4}$ the reduced order control input and the matrix obtained from $\mathbf{G}$ by removing the column $\mathbf{G}_{\flat^\star}$, respectively.

The control allocation scheme is updated, and the new task is to generate a control action able to produce the desired virtual input using the safe effectors only:

$$\breve{\boldsymbol{\tau}}_c = \breve{\mathbf{G}}_{\flat^\star} \breve{\boldsymbol{\delta}},$$

where $\breve{\boldsymbol{\tau}}_c$ has also been modified in order to compensate for the torque generated by the faulty device, i.e. $\breve{\boldsymbol{\tau}}_c = \boldsymbol{\tau}_c - \mathbf{G}_{\flat^\star} \Psi_{\flat^\star}(t, t_d)$.

To take into account for possible physical or operational limitations $(\delta_{al}, \delta_{ar}, \delta_{rl}, \delta_{rr}) \in \mathcal{Y}$, a direct control allocation method is proposed to generate the updated virtual input. Denoting by $\tau(\alpha)$ the diagonal matrix $\tau(\alpha) = diag(1, \alpha, \alpha, \alpha)$ with $\alpha \in [0, 1]$, the allocation reduces to the optimization problem

$$\max_{\alpha \in [0,1]} : \exists \breve{\boldsymbol{\delta}} \in \breve{\mathcal{Y}}_{\flat^\star} \text{ with } \breve{\mathbf{G}}_{\flat^\star} \breve{\boldsymbol{\delta}} = \tau(\alpha) \boldsymbol{\tau}_c$$

or, equivalently

$$\max_{\alpha \in [0,1]} : \breve{\boldsymbol{\delta}}_c = \breve{\mathbf{G}}_{\flat^\star}^{-1} \tau(\alpha) \boldsymbol{\tau}_c \in \breve{\mathcal{Y}}_{\flat^\star},$$

where $\breve{\mathcal{Y}}_{\flat^\star}$ is the reduced-order constraint set. The advantage of direct allocation is that, even though the inputs are saturated, their joint effect has exactly the same orientation as the desired virtual input with a possible downsized magnitude, thus reducing the risk of stall and other hazardous conditions for aircraft stability. On the other hand, in certain operational conditions, it could be preferable to give priority to generate a particulate torque rather than the others: in this case, the direct allocation can be modified choosing independently the rescaling factors, i.e. setting $\tau = (1, \alpha_1, \alpha_2, \alpha_3)$.

We notice that, if icing occurs on several effectors, the degrees of freedom in the control allocation scheme might be insufficient to guarantee a complete reconfiguration. However, performing an estimation of the loss of efficiency (see for instance [27]) allows to partially compensate for the icing effect while keeping the faulty effectors in use.

B. Airfoil leading edge icing: automated de-icing system

If ice accretion on airfoils is detected, the automated icing protection system should be turned on, this corresponding to $\iota_{iairfoil} > 0$ in (7). For example, an icing protection system is constituted of layers of coating material, a coating temperature sensor and a microcontroller, together with a thermocouple and an electric power source [5].

The coating efficiency is regulated by the microcontroller with a PID that uses the temperature as input. The ice layers detach when the coating temperature is above 0°: due to non-uniform surface temperature [28], a safety margin is imposed to ensure complete ice melting, this corresponding to a reference positive temperature $T_\star$. In particular $\iota_{airfoil}$ is an increasing function of coating temperature T and ice thickness χ with $\iota_{airfoil}(T_\star, \chi) \geq 1$ for $\chi > 0$.

VI. Case study: Aerosonde UAV

Let us consider the case study of a typical small unmanned aircraft, the Aerosonde UAV (AAI Corporation, Textron Inc.). Initial conditions for the state variables have been chosen as follows:

$$u^* = 22.95 \ m/s, \ v^* = 0.5 \ m/s \ w^* = 2.3 \ m/s$$
$$\phi^* = 0 \ rad, \ \theta^* = 0.2 \ rad, \ \psi^* = 0 \ rad$$
$$p^* = 0 \ rad/s, \ q^* = 0 \ rad/s, \ r^* = 0 \ rad/s$$

Assuming the air density $\rho = 1.2682 \ Kg/m^3$, the system matrices $\mathbf{A}$, $\mathbf{B}$ can be computed using the control and stability derivatives for the Aerosonde UAV that are reported in [16]. The icing impact coefficients $\mathcal{E}$ in the matrices

$A_{\mathcal{E}}$ and $B_{\mathcal{E}}$ can be estimated noticing that, in total icing conditions, the change in lift and drag coefficients has been experimentally observed to obey the rule [19]:

- 10% reduction of coefficients C_{Z_α}, $C_{Z_{\delta_e}}$, C_{m_α}, $C_{m_{\delta_e}}$, C_{p_β}, C_{p_p}, $C_{p_{\delta_a}}$
- 8% reduction of coefficients $C_{Y_{\delta_r}}$, $C_{p_{\delta_r}}$, C_{r_r}, $C_{r_{\delta_r}}$
- 20% reduction of coefficients C_{Y_β}, C_{r_β}

The system is supposed to be controlled by an autopilot. In the simulated scenario it keeps the airspeed constant while slowly increasing the pitch (a ramp has been considered as reference). Wind disturbances $\boldsymbol{\nu}$ have been considered, with a maximum admissible acceleration $\|\dot{\boldsymbol{\nu}}\| \leq 8m/s^2$.
Both full information and partial information cases have been considered: the observers have been designed, and to show the efficiency of the methods, sensor noise has been included in the simulation study with a covariance matrix $Q = diag[1, 1, 1, 0.01, 0.01, 0.01, 0.001, 0.001, 0.001]$. As a matter of fact, the gain matrices $\mathbf{K_1}^{(i)}$ can be chosen as to satisfy Assumption 4.1. First a fault has been supposed to affect the efficiency of the left aileron δ_{al}. Figures 1 and 2 shows the behavior of the residual $\epsilon^{(1)}$ in the full and partial information cases, respectively. Despite the presence of noise and wind disturbances, the only component to be distinctly affected by the control surfaces failure is the one in the direction $\mathbf{e}_1$: according to the decision rule, the fault can be therefore correctly identified. We notice that, in the partial information case, the size of the residual component $\mathbf{e}_1$ is even larger than in the full information case: this shows that, even though the wind effect is not completely decoupled, the method is still very sensitive to faults. Control reconfiguration is activated for $t \geq 110s$ and the nominal control action is recovered, as clearly illustrated in Figure 3, where the airspeed behavior is depicted, and in Figure 4 which represents the pitch dynamics. The second simulated scenario corresponds to incremental icing with the severity factor η slowly varying from 0 to 0.2: Figures 5 and 6 illustrate the behavior of residual $\epsilon^{(1)}$ for full and partial information cases: each of the three components $\mathbf{e}_1, \mathbf{e}_2$ and $\mathbf{e}_3$ is significantly affected by the system perturbation, this allowing to identify the anomalous effect as ice accretion on airfoils. Finally the de-icing routine has been activated, i.e. $\iota_{airfoil} > 0$ for $t \geq 70s$, and the results of icing accommodation on the airspeed are shown in Figure 7: the icing severity factor is reduced until the original performance of the system is recovered.

VII. Conclusions and future work

This paper is focused on designing an UIO-based scheme for icing detection in overactuated unmanned aerial vehicles. Decision algorithms have been proposed in order to correctly identify possibly unexpected effects in the system dynamics: wind disturbances, loss of efficiency of control surfaces and airfoil icing. Moreover the icing accommodation task is addressed, by means of a fault-tolerant control allocation scheme and exploiting input redundancy in the case of control surface failures, or by using an automated de-icing subsystem in the case of ice accretion on airfoils. Future investigations in this topic will be focused on:

- Improvement of the proposed method by including sensor fault detection.
- Generalization of the icing model and the icing detection algorithm by considering different effects on distinct portions of airfoils.

References

[1] F. Caliskan and C. Hajiyev, "A review of in-flight detection and identification of aircraft icing and reconfigurable control," *Progress in Aerospace Sciences*, vol. 60, pp. 12–34, 2013.

[2] R. W. Gent, N. P. Dart, and J. T. Cansdale, "Aircraft icing," *Phil. Trans. of the Royal Soc. of London. Series A: Mathematical, Physical and Engineering Sciences*, vol. 358, pp. 2873–2911, 2000.

[3] T. G. Myers and D. W. Hammond, "Ice and water film growth from incoming supercooled droplets," *Int. Journal of Heat and Mass Transfer*, vol. 42, pp. 2233–2242, 1999.

[4] S. Bone and M. Duff, "Carbon nanotubes to de-ice UAVs," *http://136.142.82.187/eng12/Author/data/2122.docx*, Technical report, 2012.

[5] K. L. Sørensen, A. S. Helland, and T. A. Johansen, "Carbon nanomaterial-based wing temperature control system for in-flight anti-icing and de-icing of unmanned aerial vehicles," *IEEE Aerospace Conference*, 2015.

[6] T. A. Johansen and T. I. Fossen, "Control allocation: A survey," *Automatica*, vol. 49, pp. 1087–1103, 2013.

[7] A. Cristofaro and T. A. Johansen, "Fault-tolerant control allocation using unknown input observers," *Automatica*, vol. 50, no. 7, pp. 1891–1897, 2014.

[8] J. Tjønnås and T. Johansen, "Adaptive control allocation," *Automatica*, vol. 44, pp. 2754–2766, 2008.

[9] A. Casavola and E. Garone, "Fault-tolerant adaptive control allocation schemes for overactuated systems," *Int. J. Robust and Nonlinear Control*, vol. 20, pp. 1958–1980, 2010.

[10] H. Alwi and C. Edwards, "Sliding mode FTC with on-line control allocation," *Proc. 45th IEEE Conf. on Decision and Control*, pp. 5579–5584, 2006.

[11] A. Cristofaro and T. A. Johansen, "An unknown input observer approach to icing detection for unmanned aerial vehicles with linearized longitudinal motion," in *American Control Conference (ACC),*, 2015, pp. 207–213.

[12] M. Tousi and K. Khorasani, "Robust observer-based fault diagnosis for an unmanned aerial vehicle," in *Systems Conference (SysCon), 2011 IEEE International*, 2011, pp. 428–434.

[13] A. Cristofaro, T. A. Johansen, and A. P. Aguiar, "Icing detection and identification for unmanned aerial vehicles: Multiple model adaptive estimation," in *2015 European Control Conference (ECC)*, 2015, pp. 1645–1650.

[14] D. Rotondo, A. Cristofaro, T. A. Johansen, F. Nejjari, and V. Puig, "Icing detection in unmanned aerial vehicles with longitudinal motion," in *2015 IEEE Conference on Control Applications (CCA) - Part of the 2015 IEEE Multi-Conference on Systems and Control (MSC)*, 2015, pp. 984–989.

[15] M. M. Seron, T. A. Johansen, J. A. De Dona', and A. Cristofaro, "Detection and estimation of icing in unmanned aerial vehicles using a bank of unknown input observers," in *Australian Control Conference (AuCC)*, 2015, pp. 87–92.

[16] R. Beard and T. McLain, *Small unmanned aircrafts - Theory and practice*. Princeton University press, 2012.

[17] J. Langelaan, N., Alley, and J. Neidhoefer, "Wind field estimation for small unmanned aerial vehicles," *Journal of Guidance, Control, and Dynamics*, vol. 34, no. 4, pp. 1016–1030, 2011.

[18] T. A. Johansen, A. Cristofaro, K. L. Sørensen, J. M. Hansen, and T. I. Fossen, "On estimation of wind velocity, angle-of-attack and sideslip angle of small UAVs using standard sensors," in *Intern. Conference on Unmanned Aircraft Systems (ICUAS)*, 2015, pp. 510–519.

[19] M. B. Bragg, T. Hutchinson, J. Merret, R. Oltman, and D. Pokhariyal, "Effect of ice accretion on aircraft flight dynamics," *Proc. 38th AIAA Aerospace Science Meeting and Exhibit*, 2000.

[20] T. G. Myers, "Extension to the messinger model for aircraft icing," *AIAA journal*, vol. 39, no. 2, pp. 211–218, 2001.

[21] A. Cristofaro and T. A. Johansen, "Fault-tolerant control allocation: An unknown input observer based approach with constrained output fault directions," *Proc. 52nd IEEE Conf. on Decision and Control*, pp. 3818–3824, 2013.

[22] C. Hajiyev and F. Caliskan, *Fault diagnosis and reconfiguration in flight control systems*. Springer Science & Business Media, 2003.
[23] D. Wang and K.-Y. Lum, "Adaptive unknown input observer approach for aircraft actuator fault detection and isolation," *Int. J. of Adaptive Control and Signal Processing*, vol. 21, no. 1, pp. 31–48, 2007.
[24] J. Park and G. Rizzoni, "An eigenstructure assignment algorithm for the design of fault detection filters," *IEEE Transactions on Automatic Control*, vol. 39, no. 7, pp. 1521–1524, 1994.
[25] Y. Zhang, S. Suresh, B. Jiang, and D. Theilliol, "Reconfigurable control allocation against aircraft control effector failures," *Proc. 16th IEEE Conf. on Control Applications*, pp. 1197–1202, 2007.
[26] A. Cristofaro and T. A. Johansen, "Fault-tolerant control allocation with actuator dynamics: finite-time control reconfiguration," *Proc. 53rd IEEE Conf. on Decision and Control*, pp. 4971–4976, 2014.
[27] A. Cristofaro, M. M. Polycarpou, and T. A. Johansen, "Fault diagnosis and fault-tolerant control allocation for a class of nonlinear systems with redundant inputs," in *Proc. 54th IEEE Conf. on Decision and Control*, 2015, pp. 5117–5123.
[28] K. L. Sørensen and T. A. Johansen, "Thermodynamics of a carbon nano-materials based ice protection system for unmanned aerial vehicles," in *IEEE Aerospace Conference*, 2016.

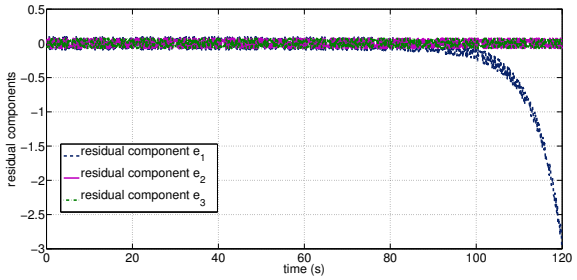

Fig. 1. Faulty aileron δ_{al}: components $\mathbf{e}_1, \mathbf{e}_2$ and $\mathbf{e}_3$ of residual $\epsilon^{(1)}$ (full information case).

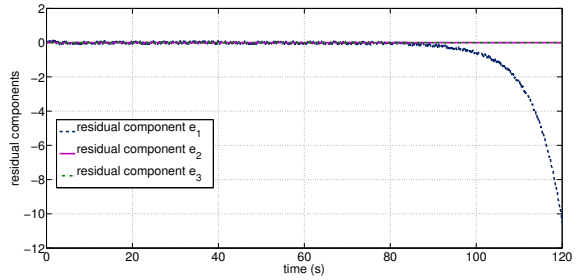

Fig. 2. Faulty aileron δ_{al}: components $\mathbf{e}_1, \mathbf{e}_2$ and $\mathbf{e}_3$ of residual $\epsilon^{(1)}$ (partial information case).

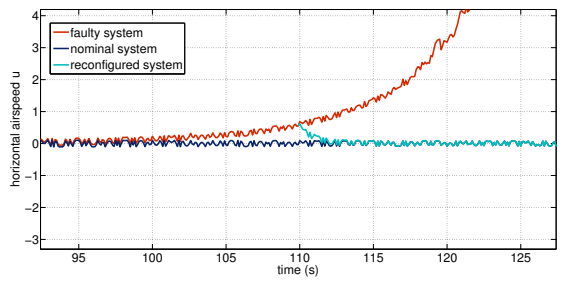

Fig. 3. Horizontal airspeed u: faulty system, nominal system, reconfigured system

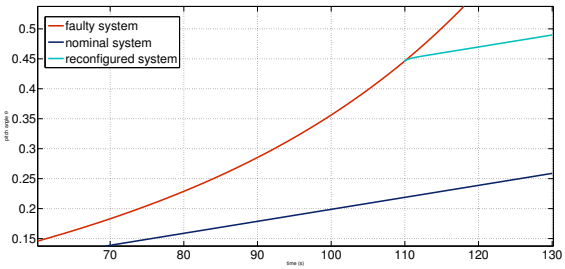

Fig. 4. Pitch θ: faulty system, nominal system, reconfigured system

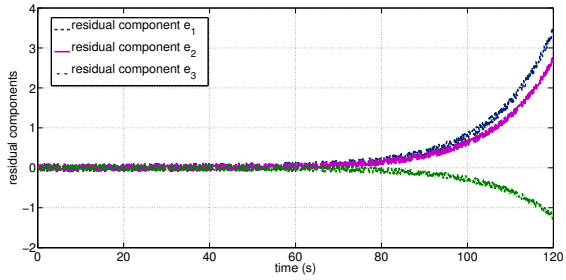

Fig. 5. Incremental airfoil icing: components $\mathbf{e}_1, \mathbf{e}_2$ and $\mathbf{e}_3$ of residual $\epsilon^{(1)}$ (full information case).

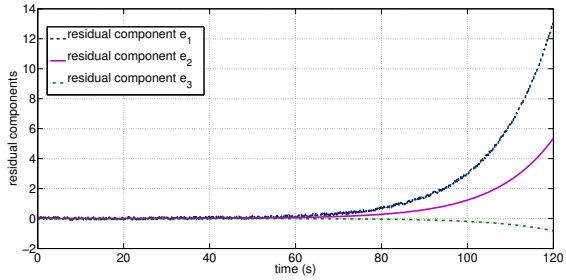

Fig. 6. Incremental airfoil icing: components $\mathbf{e}_1, \mathbf{e}_2$ and $\mathbf{e}_3$ of residual $\epsilon^{(1)}$ (partial information case).

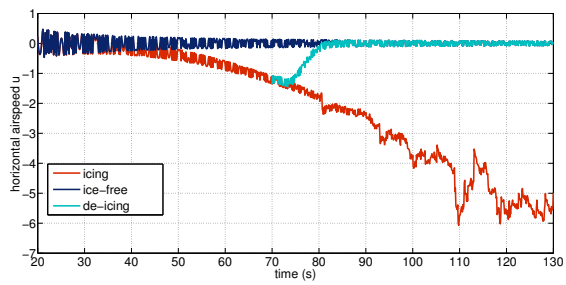

Fig. 7. Horizontal airspeed u: system with ice accretion, nominal system (ice-free), activation of automated de-icing system